Contents lists available at ScienceDirect

Renewable Energy

journal homepage: http://ees.elsevier.com

Solar thermal performance of two innovative configurations of air-vacuum layered triple glazed windows

Yueping Fang [a,*], Saim Memon [b], Jingqing Peng [c], Mark Tyrer [a], Tingzhen Ming [d]

[a] Coventry University, Centre for Research in Built and Natural Environment, School of Energy, Construction and Environment, Priory Street, Coventry, CV1 5FB, UK
[b] London South Bank University, London Centre for Energy Engineering, School of Engineering, 103 Borough Road, London, SE1 0AA, UK
[c] Hunan University, Key Laboratory of Building Safety and Energy Efficiency of the Ministry of Education, Changsha, 410082, PR China
[d] Wuhan University of Technology, School of Civil Engineering and Architecture, 122 Luoshi Road, Hongshan District, Wuhan, 430070, PR China

ARTICLE INFO

Article history:
Received 16 August 2019
Received in revised form 20 December 2019
Accepted 24 December 2019
Available online xxx

Keywords
Vacuum
Window
Solar insolation
Thermal performance
Low emittance coatings

ABSTRACT

This study reports the optimal solar thermal performance of two innovative configurations of air-vacuum layered triple glazed window or Integrated Vacuum Window (IVW). These are when the vacuum layer of IVW is facing the warm or indoor side, i.e. IVW_{warm}, and when the vacuum layer of IVW is facing the cold or outdoor side, i.e. IVW_{cold}, positions at dynamic solar insolation under winter and summer EN-ISO standard ambient conditions. A theoretically and experimentally validated finite element model is employed. The results show that in winter conditions, although the U-value of IVW_{warm} of 0.33 $Wm^{-2}K^{-1}$ is lower than that of IVW_{cold} of 0.49 $Wm^{-2}K^{-1}$, the IVW_{cold} has a higher solar heat gain. In sunny winter conditions, IVW_{cold} provides higher energy efficiency while in winter night, IVW_{warm} provides higher energy efficiency than IVW_{cold}. The results show that in summer conditions the U-value of IVW_{warm} and IVW_{cold} are 0.34 $Wm^{-2}K^{-1}$ and 0.51 $Wm^{-2}K^{-1}$ respectively, while IVW_{warm} provides lower cooling-load and higher energy-efficiency compared to IVW_{cold}. It is concluded that setting the vacuum gap at the indoor side position provides lower cooling-load and higher energy-efficiency compared to setting the vacuum cavity at the outdoor side position in summer ambient conditions.

1. Introduction

A significant rise of the sustainable development of buildings [1] with a goal of Nearly Zero-Energy Building (NZEB) [2] is emerged by merging the progressive technologies of PV, Wind and optimal building fabric insulation with a future leading to the idea of Generating-Energy Building (GEB). To achieve this long-term sustainable development goal, a number of retrofitting measures have already been reported [3] and it is found that usually the windows exhibit poorer thermal performance [4] and poorer sound insulation among other components since windows need to allow the sunlight get into the rooms and the occupants to view outside. Heat loss through windows take place by conductive, convective and radiative heat transfers [5]. Multiple glass sheets with an air or inert gas filled gap, enclosing the air and inert gas in between, can reduce the conductive heat loss across the glazing. Low-emittance (low-e) coatings can be applied to the inner surfaces between two sheets of glass to decrease the radiative heat transfer between these two inner surfaces [6,7]. The width of gas-filled gap(s) requires typically about 10 mm, otherwise the contribution of heat transfer resulting from gas conduction and convection will compromise the thermal insulation of the gas-filled window [8]. The multiple glass sheets with gas-filled gaps increases the thickness and weight as well as reduce the light transmission. Vacuum glazed window overcomes these difficulties [9]. Vacuum glazed window combines the merits of lower thermal transmittance (U value) < 1 $Wm^{-2}K^{-1}$ with higher solar heat gains (g-value > 0.76) whilst maintaining the visual light transmittance of about 0.74 [10]. It comprises an evacuated cavity between two glass sheets sealed contiguously along their perimeter. Low-emissivity coatings are coated onto either one or two inner glass surfaces inhibit long-wave radiation. The vacuum pressure of 0.1 Pa within the vacuum cavity enclosed by the two sheets of glass is achieved by evacuating with specialised made vacuum cup connected to the turbo-molecular vacuum pump [11,12], it reduces the thermal conduction and convection to minimum level except the heat transfer via support pillars and edge seal. The edge seal width of air-filled layer and vacuum layer are 10 mm and 0.12 mm respectively. However, the vacuum glazing adds the benefits of a very small gap can be integrated to the conventional air-filled glazing with the existing window frames for the retrofit as well as for new window frames [4].

The first successful vacuum glazing [13] utilises high-temperature sealing material, lead-based solder glass from Schott Glass company [14], to seal the edges hermetically at 450 °C. The group at the Ulster University developed the successful low-temperature edge sealing method (160 °C), utilising indium-alloy [6], to seal the edges of the

* Corresponding author.
E-mail address: yueping.fang@coventry.ac.uk (Y. Fang)

https://doi.org/10.1016/j.renene.2019.12.115
0960-1481/

glass sheets and added benefits of incorporated low-e coatings and the use of tempered glass. Since then, a significant development has been made in the vacuum edge sealing materials for the fabrication and development of vacuum glazing and triple vacuum glazing [15,16]. Fang et al. (2014) [4] has shown that vacuum glazing can be fabricated at temperatures around 160 °C, thus removing the thermal restriction on the use of tempered glass [17]. Thus, subject to outgassing characteristics, the full range of optical glazing properties currently seen in gas filled glazing may also be possible with evacuated cavities. Although significant efforts have been made by many researchers [18,19], the U-value of the vacuum glazing has been reduced close to the theoretical limits. To meet the demand of Nearly Zero-Energy Buildings, triple vacuum glazing (TVG), hybrid vacuum glazing (HVG) and Integrated Vacuum Window (IVW) can further improve the window performance. The difference between HVG and IVW is that HVG uses argon gas and does not account the frame whilst IVW does use air and account the frame. Preliminary research have been undertaken by the researchers [15,20]. The predicted U-values of TVG and HVG have been experimentally validated [21].

Recently, there has been an increasing mass production, such as Qingdao Hengda Vacuum Glass Ltd [22], LandVac Ltd. [23], and Panasonic Ltd [24], and installation of vacuum glazing in Nearly Zero-Energy Buildings in China and Japan. The NSG SPACIA Hybrid vacuum glazing [25] utilises the argon gas filled layer and solder-glass based vacuum glazing and there have been issues of argon gas leakage and its added complexity of the secondary edge seal. In this paper, air-vacuum layered triple glazed window is developed with low-temperature (indium-alloy) edge seal for vacuum layer and butyl rubber seal for air-filled layer, named as Integrated Vacuum Window (IVW), that added the benefits of incorporating the low-e coatings and temperature sensitive heat-reflective coatings. This paper offers for the first time, current industrial knowledge gap, of understanding the optimal indoor(warm-side)/outdoor (cold-side) position of the vacuum layer of IVW under winter and summer ambient EN-ISO conditions at dynamic solar insolation for the greater benefit in terms of maintaining the durability and longevity of vacuum edge-seal, the position of vacuum layer in IVW, a possibility of reducing the condensation issue by reducing the edge effects and additional temperature differential based internal and external tensile stresses. This paper also reports the solar thermal performance of IVW subjected by various solar insolation under EN-ISO winter and summer ambient conditions [8,26]. The optimal setting method of IVW is presented based on the analysis using validated [7] finite element model.

2. Methodology

Integrated Vacuum Window (IVW), as shown in Fig. 1, comprises three glass sheets, each dimensions of 400 mm × 400 mm x 4 mm, having a layer of air-filled gap and a layer of vacuum gap supported with a wooden frame. The advantages of IVW as compared to the low-temperature indium-alloy sealed vacuum glazing (VG) are: i) its U-value is lower than VG due to the added air gap, which contributes to the added thermal resistance within the IVW; ii) the stress within the VG is significantly reduced, since the added air gap enclosed by the 3rd glass sheet reduces the temperature deferential between the two sheets of glass of IVW, thus improving the durability and longevity of the vacuum layer; iii) the third glass sheet and the air gap, reduce the risk of condensation at the edge seal area of the Vacuum layer due to the thermal bridge of the edge seal. The thermal performance of IVW has been analysed using an experimentally validated finite element model (FEM) [7,10,21] in which the solar thermal performance of IVW with different positions of the vacuum layer subjected to various levels of solar insolation were investigated in this work.

2.1. Analytic model of Integrated Vacuum Window (IVW)

An analytic heat transfer model for IVW has been established following experimentally and theoretically validated approach of [7,10,21]. Due to the geometrical symmetry of the IVW and to reduce the computational time, one-fourth of the IVW is modelled. The equivalent thermal resistive network for the one-fourth of a support-pillar,

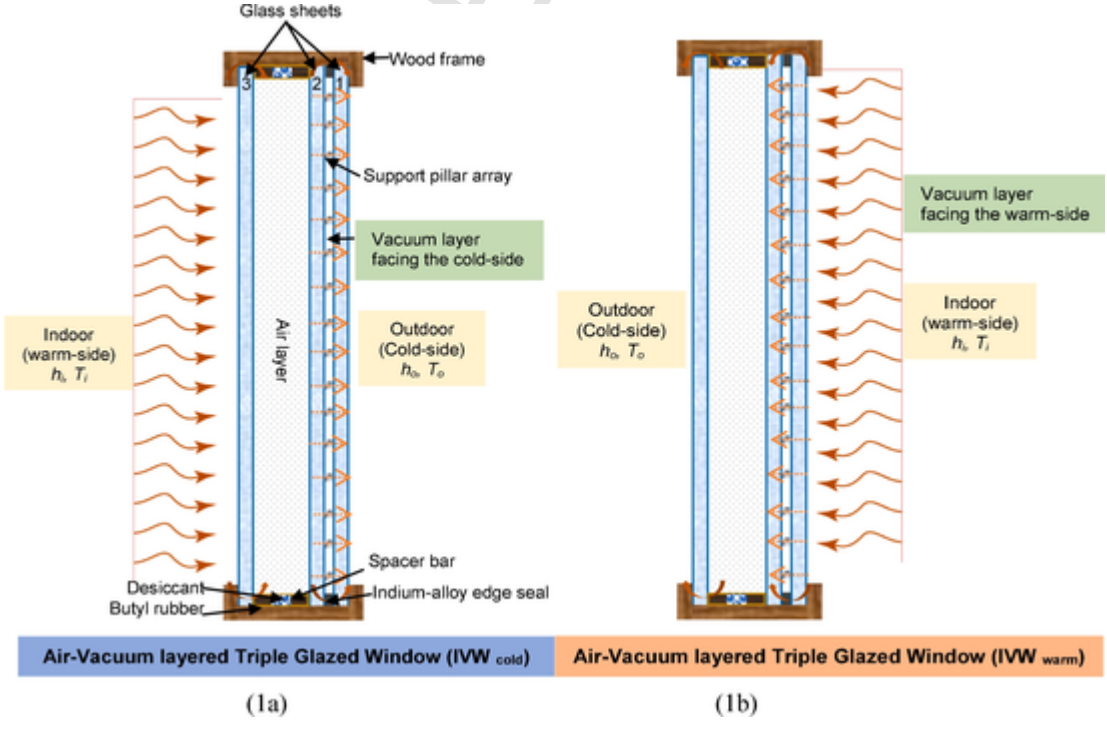

Fig. 1. Schematic diagram of air-vacuum layered triple glazed window in which vacuum layer is facing the EN-ISO ambient conditions of: (1a) outdoor (cold-side) named as (IVW $_{cold}$) and (1b) indoor (hot-side) named as (IVW $_{warm}$). (The diagram is not to scale).

due to the symmetry of the circular shape of the support-pillar, and to reduce the computational time one quarter of the IVW is modelled and is consistent to the validated approach, as shown in Fig. 2.

The overall thermal resistance across the IVW is determined by Eq. (1),

$$R_{total} = \frac{R_p\left(R_{g,1} + R_{r,1} + \frac{1}{2}R_{g,2}\right)}{R_p + R_{g,1} + R_{r,1} + \frac{1}{2}R_{g,2}} + \frac{1}{2}R_{g,2} + R_{air-layer} + R_{g,3} \quad (1)$$

Where R_p is the thermal resistance of the support pillar, determined by Eq. (2) [13].

$$R_p = \frac{1}{2\lambda_g a} \quad (2)$$

$R_{g,1}$, $R_{g,2}$, $R_{g,3}$ are thermal resistances of three glass sheets 1, 2 and 3, determined by Eq. (3),

$$R_{g,m} = \frac{d_m}{\lambda_g A} \quad (3)$$

where d_m is the glass thickness; m is either *I,* or *II,* or *III*; a is support pillar's radius; A indicates the unit cell area (so $A = p^2$); λ_g is glass thermal conductivity.

The thermal resistance against radiative heat transfer between the two inner surfaces of glass panes enclosing the air filled gap and vacuum cavity is given by Eq. (4).

$$R_{r,n} = \left(\frac{1}{\varepsilon_x} + \frac{1}{\varepsilon_y}\right)\left(4\sigma T_{xy}^3 A\right)^{-1} \quad (4)$$

In the equation ε_x and ε_y indicate the atmospheric emittance of two inner surfaces x and y within the vacuum cavity and air filled gap; T_{xy} is the mean temperature of the two sheet of glass enclosing either the vacuum gap or the air filled gap; σ stands for Stefan-Boltzmann constant.

The thermal resistance of the air filled gap $R_{air,gap}$ is computed by the thermal resistance R_{air} against conductive and convective heat flow across the air filled gap and the thermal resistance R_r against radiative heat flow within the air gap enclosed by two sheet of glass, i.e.

$$R_{air,gap} = \frac{R_{air}R_{r,2}}{R_{air} + R_{r,2}} \quad (5)$$

$$R_{air} = \frac{1}{Ah_{air,gap}} \quad (6)$$

The British and European standard BS EN 673 [26] recommends that

$$h_{air} = Nu\frac{k}{l} \quad (7)$$

Here, l is the air gap width; Nu indicates the Nusselt number; k indicates the air thermal conductivity:

$$Nu = K \cdot (Gr \cdot \mathrm{Pr})^n \quad (8)$$

In Eq. (8), K is a constant; n: an exponent; Pr: the Prandtl number; Gr: the Grashof number;

$$Gr = \frac{9.81 s^3 \Delta T \cdot \rho^2}{T_a \mu^2} \quad (9)$$

$$P_r = \frac{\mu c}{k} \quad (10)$$

Here, ΔT stands for the temperature differential between surfaces 2 and 3 in Fig. 1(a) and surfaces 4 and 5 in Fig. 1(b) of the air gap. For the air in the air gap, μ is the dynamic viscosity; T_a: the mean temperature of the two inner surfaces of sheet of glass enclosing the air gap; c: the specific heat capacity; ρ: the density. If Nu is less than 1, then the Nu number is selected to be 1. For air gap between the two vertical glass sheets: K is chosen to be 0.035, n chosen to be 0.38 [26]. The R_i and R_o are thermal resistance of the indoor and outdoor surface of IVW. The overall U-value of the IVW is then determined by Eq. (11).

$$U_{a-a,tot} = \frac{1}{\left(R_i + R_{tot} + R_o\right)A} \quad (11)$$

The heat flow across the whole IVW is calculated by adding the heat flow through the central section of IVW with the heat transfer across the edge seal of the vacuum cavity and the spacer of air filled gap.

2.2. Finite element model

The validated boundary conditions for the finite element model are detailed as follows:

a) The overall heat loss coefficients of the outdoor and indoor surfaces of IVW are h_o = 25 $Wm^{-2}K^{-1}$ and h_i = 7.7 $Wm^{-2}K^{-1}$ [8].
b) The temperatures of outdoor and indoor ambient are 0 °C and 20 °C respectively [8].

The Galerkin approach was used to discretize and solve the governing equation. The radiation between the two parallel surfaces of the finite element brick within the vacuum and air gaps is determined by Eq. (12).

$$dQ_r = \left(\frac{1}{\varepsilon_j} + \frac{1}{\varepsilon_k} - 1\right)^{-1}\left(4\sigma T_{j,k}^3 dA_v\right)\left(T_j - T_k\right) \quad (12)$$

Here, dA_v is determined by Eq. (13).

$$dA_v = dxdy \quad (13)$$

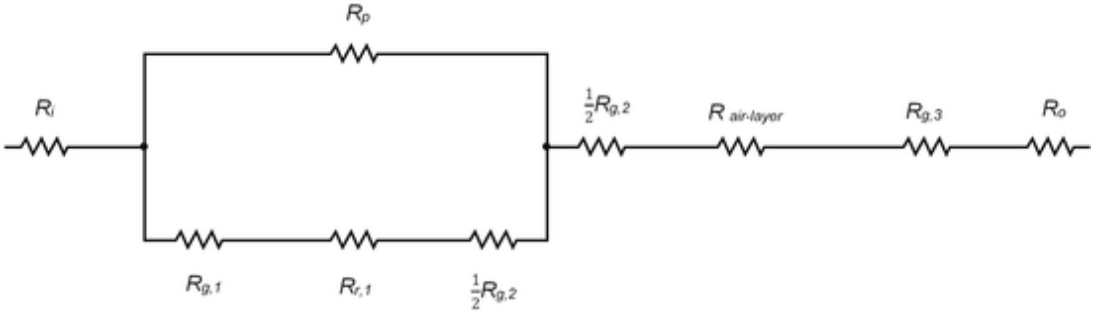

Fig. 2. An equivalent thermal resistance circuit diagram of the quarter cell unit with a quarter of a pillar at the symmetric centre of the unit.

The dQ_r was integrated with the conductive heat transfer across the support pillar in the vacuum cavity and the air-filled gap. The heat flow across the air-filled gap was simplified to the heat conduction through an equivalent material with an effective thermal conductivity [27] determined by Eq. (14) which is the effective air gap thermal conductivity.

$$k = \frac{s}{A_g R_{air,gap}} \tag{14}$$

Here, s is the air gap width and A_g is the glass sheet area.

The circular support pillars with diameter of a are integrated into the model as a cubic pillar with width of $\sqrt{\pi}a$ and with the physical properties of stainless [10–12]. The area (cross-sectional) of the circular pillar and cubical pillar are same, and therefore conduct same amount of heat under the same ambient conditions [15]. The mesh numbers within and around the pillar are denser to achieve higher accuracy than that of the area distance away from the pillars to reduce the CPU running time [7].

The edge spacer and butyl rubber seal of double glazing was simplified as a single equivalent materials with effective thermal conductivity of 0.16 $Wm^{-2}K^{-1}$ that was determined by a 2-D finite element model detailed by Refs. [10,21].

Solar energy absorption in each finite volume is shown in Fig. 3 and is given by Eq. (15).

$$dI_{absorbed} = I_{in}\left(I_Z - I_{Z+1}\right)dxdy \tag{15}$$

where I_z and I_{z+1} are the solar insolation intensities at the up and bottom surfaces of each finite element, which was given by Eq. (16).

$$I_L = 1 - e^{-C_e Z_L} \tag{16}$$

where the glass extinction coefficient, C_e is a parameter indicating the amount the glass absorbs solar radiation [28]. It has been reported that the extinction coefficient of "greenish edge" glass is 32 m^{-1} and that of "white edge" glass is 4 m^{-1}. In this finite volume model, C_e was selected to be 30 m^{-1}. Z_L is the length of the sun light passing within the IVW from the outdoor glass surface.

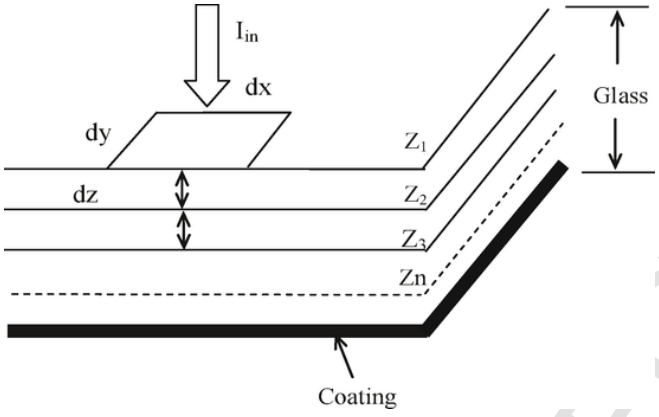

Fig. 3. Schematics of an enlarged finite element volume within the glass sheet. The diagram is not to scale.

3. Results and discussion

3.1. Solar thermal performance of IVW under EN-ISO winter boundary conditions

The isotherms of IVW_{warm} and IVW_{cold} settings, as shown in Fig. 1, under standard winter ambient conditions [8] with solar insolation of 0 W/m^2 and 300 Wm^{-2} are presented in Fig. 4 and Fig. 5.

In Fig. 4 with solar insolation of 0 Wm^{-2}, the temperatures at the central glazing area of IVW_{warm} and IVW_{cold} are 12.6 °C and 11.1 °C. Their U-values are 0.33 $Wm^{-2}K^{-1}$ and 0.49 $Wm^{-2}K^{-1}$ respectively. The vacuum cavity at the indoor warm side of the middle glass reduces the heat transfer more effectively than that at the cold outdoor side. The air gap at the indoor side of the middle glass exhibits higher thermal conductance compared to that when the air gap is at the outdoor low temperature side, since higher temperature at the indoor warm side leading to a higher heat convection within the air gap. This means that at night or on overcast winter days, IVW_{warm} provides better insulation than IVW_{cold}, i.e. less heat loss.

Figs. 4(a) and 5(a) show that with solar insolation increasing from 0 to 300 Wm^{-2}, the temperature at the centre of the indoor warm side glass of IVW_{warm} increases from 12.6 °C to 25.5 °C; while in Figs. 4(b) and 5(b), the temperatures of the central glazing section of the

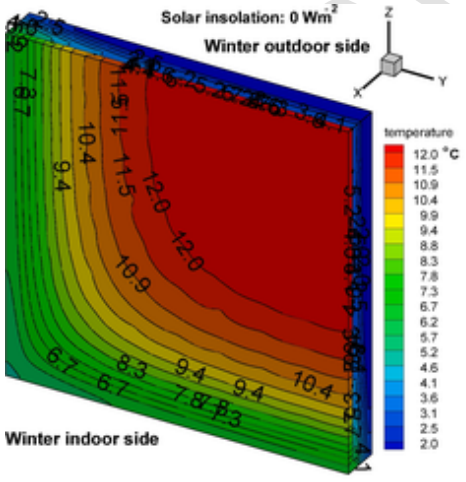

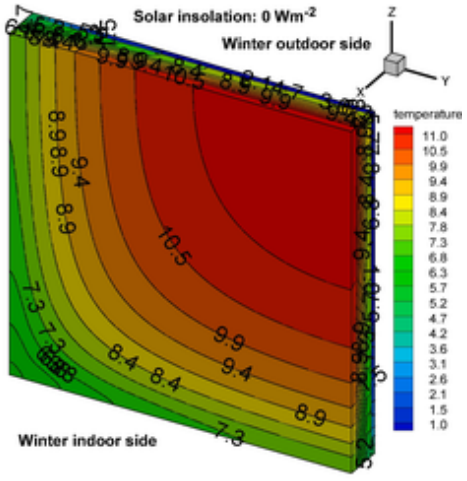

(4a) (4b)

Fig 4. 3D Isotherms of (4a) IVW_{warm} with the vacuum cavity at the indoor (warm-side) and (4b) IVW_{cold} with the vacuum cavity at the outdoor (cold-side) at the solar insolation of 0 W/m^2.

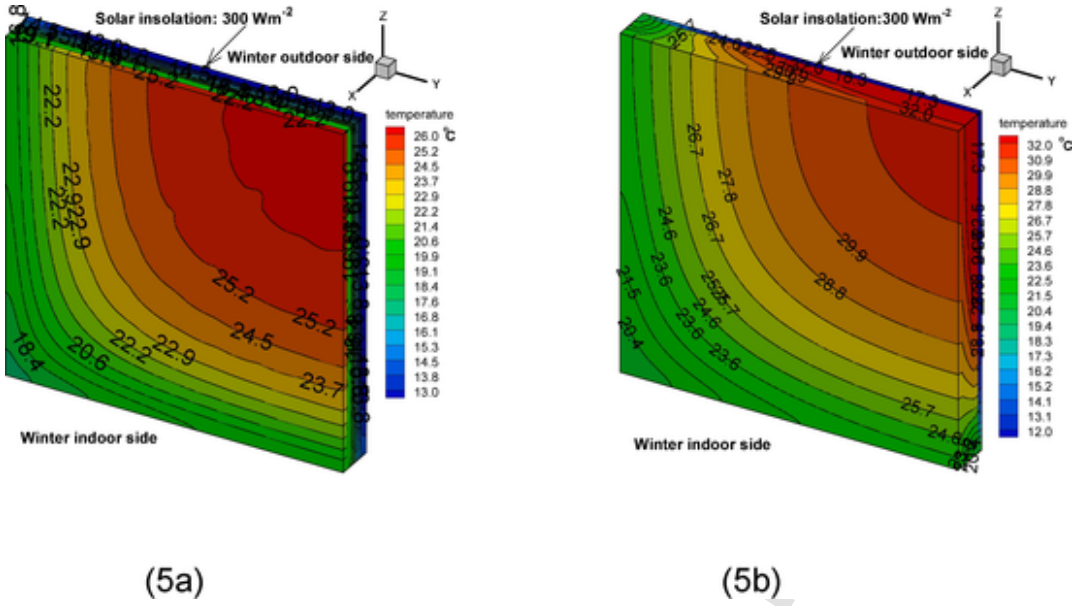

Fig 5. 3D Isotherms of (5a) IVW_{warm} with the vacuum cavity at the indoor (warm-side) and (5b) IVW_{cold} with the vacuum cavity at the outdoor (cold-side) at the solar insolation of 300 W/m^2.

indoor glass sheet of IVW_{cold} increases from 11.1 °C to 30.4 °C, i.e. the temperature increase in the indoor glass of IVW_{cold} is higher than that of IVW_{warm}. This is because in IVW_{cold}, the vacuum cavity at the cold side provides better insulation compared to that when the air gap is at the cold side as in IVW_{warm}, thus reduces the heat transfer from the middle sheet of glass to the sheet of glass at the cold side more effectively compared to that in IVW_{warm} with the vacuum cavity being at the warm side. This means that subjected to solar insolation, IVW_{cold} transfers more heat into the warm ambient side, given the temperature of indoor side glass is over the indoor ambient temperature and thus has a higher solar heat gain than IVW_{warm}.

Figs. 4 and 5 also show that the temperatures of the indoor glass edge area is lower compare to that at the area of central glazing, because more heat is transferred by conduction across the seal of vacuum cavity and the spacer of air gap from the warm indoor environment to the outdoor environment compared to the heat flow across the central window area because of higher insulation of the vacuum cavity.

The temperature variations of three glass sheets of IVW_{warm} and IVW_{cold} subjected to various levels of solar radiation were calculated by using the validated FEM model as shown in Fig. 6.

Fig. 6(a) shows an increase of solar insolation higher than 210 W/m^2, the indoor glass temperature T_3 is higher compared to indoor ambient temperature T_i of 20 °C and middle glass sheet temperature T_2, the warm-side glass sheet transfers heat onto both the warm-side ambient air and into the middle sheet of glass and then to the glass sheet at the cold side. Fig. 6(b) shows that with an increase of solar insolation, the middle glass sheet temperature T_2 is increased faster than that of indoor glass sheet temperature T_3; T_2 becomes higher than T_3 when the solar insolation increases to 200 W/m^2 since the heat absorbed from solar energy is difficult to transfer to the outdoor glass sheet because of the lower thermal conductance of the vacuum cavity at the outdoor side. Heat flows from the middle sheet of glass to the indoor sheet of glass, then to the indoor warm ambient, due to the indoor glass temperature being higher compared to the indoor ambient temperature.

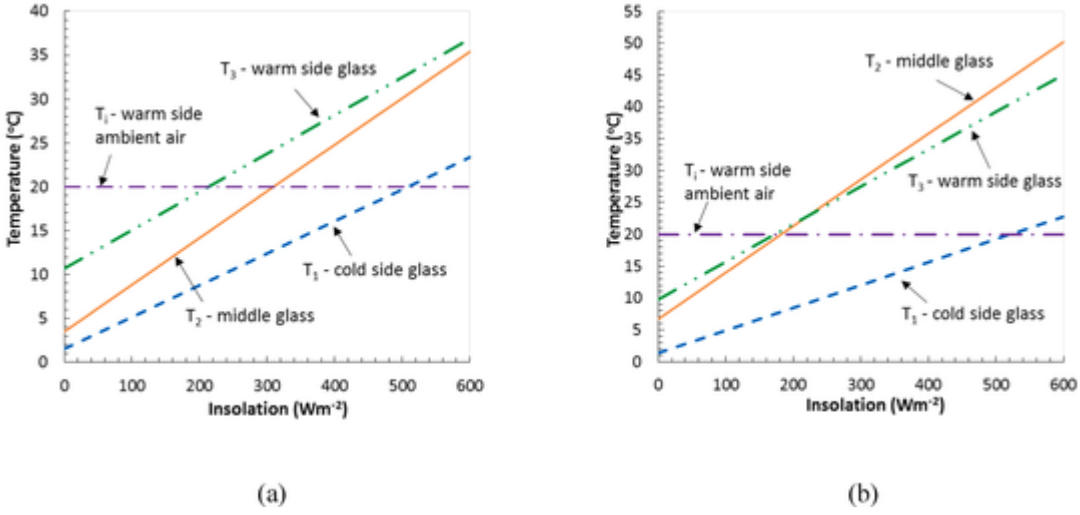

Fig. 6. Surface Temperatures in relation to dynamic solar insolation of (6a) IVW_{warm} and (6b) IVW_{cold}.

3.2. Solar thermal performance of IVW under EN-ISO summer boundary conditions

The employed summer boundary conditions for the finite element model are listed as follows: the overall heat loss coefficients of the outdoor and indoor IVW surfaces are h_o = 25 $Wm^{-2}K^{-1}$ and h_i = 7.7 $Wm^{-2}K^{-1}$; the outdoor and indoor ambient temperature: 37 °C and 22 °C [8]. The isotherms of IVW_{warm} and IVW_{cold} without solar insolation and with insolation of 300 W/m^2 are presented in Fig. 7 and Fig. 8.

Fig. 7 shows that with solar insolation of 300 W/m^2, the temperatures at the centre of the indoor (cold-side) glass sheets of IVW_{warm} and IVW_{cold} are 27.7 °C and 29.5 °C. Their U-values are 0.34 $Wm^{-2}K^{-1}$ and 0.51 $Wm^{-2}K^{-1}$ respectively. The vacuum cavity at the indoor cool side of the middle glass of IVW_{warm} reduces the heat transfer more effectively than that when the vacuum cavity is at the outdoor warm side of the middle sheet of glass. The heat absorbed by the middle sheet of glass cannot transfer into the indoor glass sheet due to high insulation of vacuum cavity of IVW_{warm}. For IVW_{cold}, the heat absorbed by the middle sheet of glass can easily transfer into the indoor glass due to higher thermal conductance of air gap at the indoor side of middle glass sheet. Thus, the temperature of indoor glass of IVW_{cold} is higher compared to that of indoor sheet of glass of IVW_{warm}, resulting in the temperature of indoor sheet of glass of IVW_{cold} being higher compared to that of IVW_{warm}.

Figs. 7(a) and 8(a) show that an increase of solar insolation from 0 to 300 W/m^2, the temperature of the indoor central glazing area of IVW_{warm} increases from 27.7 °C to 40.0 °C, whilst in Figs. 7(b) and 8(b), the temperatures of the central glazing section of the indoor

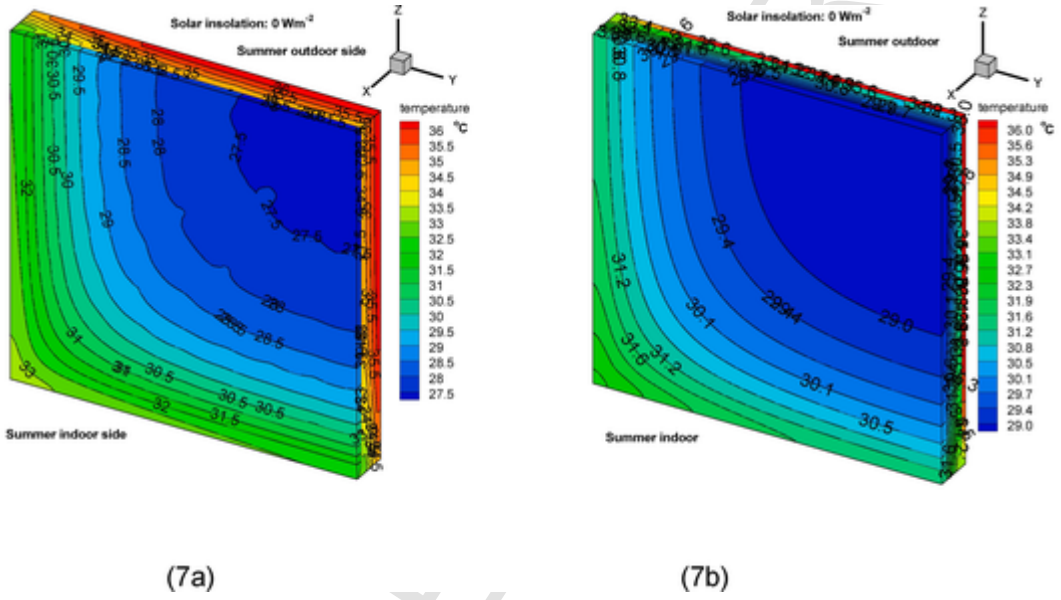

Fig 7. 3D Isotherms of (7a) IVW_{warm} with the vacuum cavity at the indoor (warm-side) and (7b) IVW_{cold} with the vacuum gap at the outdoor (cold-side) at the solar insolation of 0 W/m^2.

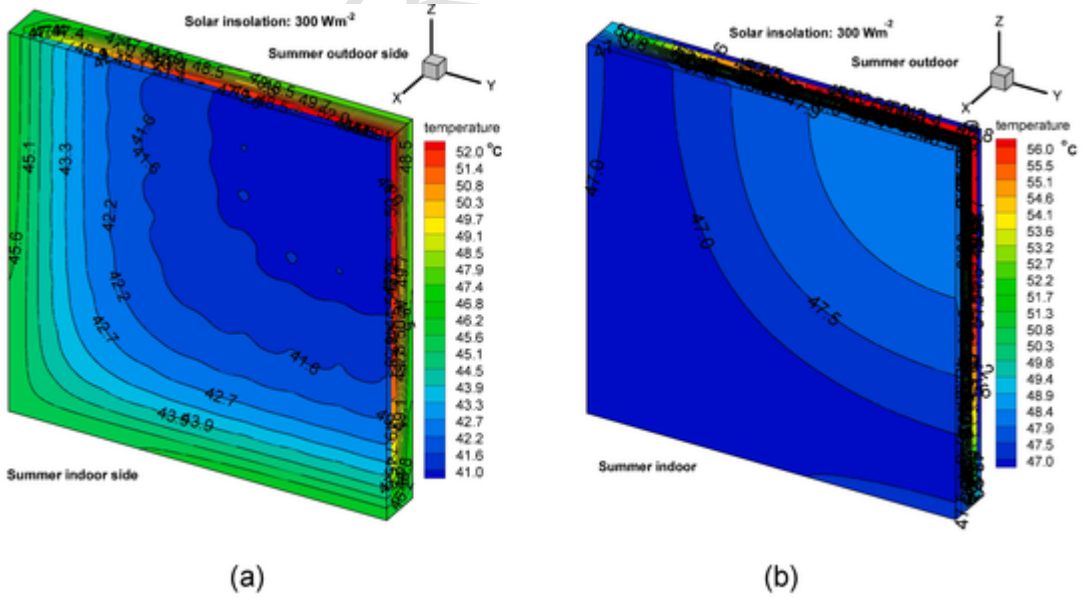

Fig 8. 3D Isotherms of (8a) IVW_{warm} with the vacuum cavity at the indoor (warm-side) and (8b) IVW_{cold} with the vacuum cavity at the outdoor (cold-side) at the solar insolation of 300 W/m^2.

cooler glass of IVW_{cold} increases from 29.5 °C to 47.0 °C, i.e. the increase in temperature of the indoor (cold-side) glass sheet of IVW_{cold} is higher than that of IVW_{warm}. This is because in IVW_{cold}, the vacuum gap at the outdoor side provides better insulation than the air gap at the outdoor side as in IVW_{warm}, thus decreases the heat flow from the middle sheet of glass to the outdoor environment more effectively compared to that in IVW_{warm}. This causes the temperature of the indoor sheet of glass increasing faster than that when the vacuum gap is at the indoor side of the middle glass sheet of IVW_{warm}, thus IVW_{cold} transfers more heat into the indoor ambient than IVW_{warm}, providing a higher solar heat gain than IVW_{warm}, leading to a higher cooling load compared to IVW_{warm}.

Figs. 7 and 8 also show that the temperature of the indoor sheet of glass near the edge area is higher than that of central glazing area, since more heat is conducted vie both the seal of vacuum cavity and spacer of the air gap from the warm outdoor environment compared to the heat flow across the central window area because of higher insulation of the vacuum cavity.

The temperature variations of three glass sheets of IVW_{warm} and IVW_{cold} subjected to various levels of solar radiation were determined using the FEM as shown in Fig. 9.

Fig. 9(a) shows that when the solar insolation is higher than 60 W/m^2, the surface temperature T_2 of the middle glass sheet is taking over temperature T_1 of indoor side glass thus the heat absorbed by the middle glass transfers to the outdoor glass, then to the outdoor ambient environment across the air gap. Because of the high insulation of the vacuum cavity at the indoor side, the heat absorbed by the middle glass sheet transfers into the indoor environment at a much lower rate than that into the outdoor environment. In a move to Building Integrated PV technology, if semi-transparent PV cells were to be incorporated then they should be set onto the indoor (warm-side) of the glass sheet enclosing the vacuum gap, since indoor glass temperature T_3 is lower than that of outdoor glass temperature T_1.

Fig. 9(b) shows that when the solar insolation is higher than 110 W/m^2, the middle glass temperature T_2 is higher than the outdoor glass sheet temperature T_1, thus the heat absorbed by the middle glass transfers into the outdoor environment across the vacuum gap, but at a much lower rate than that transfers into the indoor environment across the air gap. IVW_{cold} exhibits a much higher solar heat gain g-value and a higher cooling load than IVW_{warm}. With insolation increasing to 220 W/m^2, temperature T_3 of the indoor glass is taking over temperature T_1 of outdoor glass, transferring the heat to both indoor ambient and the outdoor glass sheet, then to the outdoor ambient environment.

In summary, the position that the vacuum layer facing the indoor (warm-side) of the middle glass sheet provides a lower cooling load and higher energy efficiency compared to setting the vacuum cavity at the outdoor side of the middle glass sheet in summer ambient conditions.

4. Conclusions

Thermal performance of IVW subjected to various levels of solar insolation were simulated using a validated finite volume model that has been experimentally and theoretically validated by the previous work. The results show that in the winter EN-ISO ambient condition IVW_{cold} exhibits a larger solar heat gain g-value, transferring more heat into the warm indoor environment, despite the fact that the U-value of IVW_{warm} with the vacuum cavity at the indoor side of the middle sheet of glass being lower than that of IVW_{cold} with the vacuum gap at the cold side. It is concluded that at the IVW_{cold} setting at which the vacuum layer facing the cold-side is preferred during winter daytimes with sufficient solar insolation. However, IVW_{warm} with a lower U-value exhibits better thermal performance during winter nights, i.e. lower heat loss compared to IVW_{cold}. Thus, IVW with a pivotal axial that enables rotation of the window during winter daytime and nighttime may provide optimized energy saving potential.

Detailed analysis for the energy balance of IVW at different locations on the earth is required to achieve maximized energy efficiency of IVW. For instance, in areas with long winter nights or with short sunny days, IVW_{warm} is better than IVW_{cold} since IVW_{warm} has lower U-value than IVW_{cold}; while in areas where g-value dominates the energy balance, IVW_{cold} is better than IVW_{warm} since IVW_{cold} has a higher g-value than IVW_{warm}, even if the U-value of IVW_{cold} is higher than that of IVW_{warm}.

In summer EN-ISO boundary conditions, it is concluded that IVW_{warm} provides lower cooling load compared to IVW_{cold}, since the vacuum gap at the outdoor side of the middle glass sheet of IVW_{cold} more efficiently prevents the heat absorbed by the middle glass sheet transferring into the outdoor ambient compared to the case when vacuum gap is at the indoor side of the middle glass sheet. Thus, IVW_{cold} provides higher solar heat gain compared to IVW_{warm}, which will increase the cooling load of the room in summer.

As for the future work recommendation, it is pertinent to mention the scope of integrating the Semi-Transparent PV (STPV) cell into IVW. In this case, the results of this paper implicate that STPV should then be set on the external glass sheet of the IVW enclosing the vacuum gap. In this case, the STPV would face the outdoor (cold-side) of IVW_{cold} in winter. During this time period, IVW_{cold} achieves higher solar heat

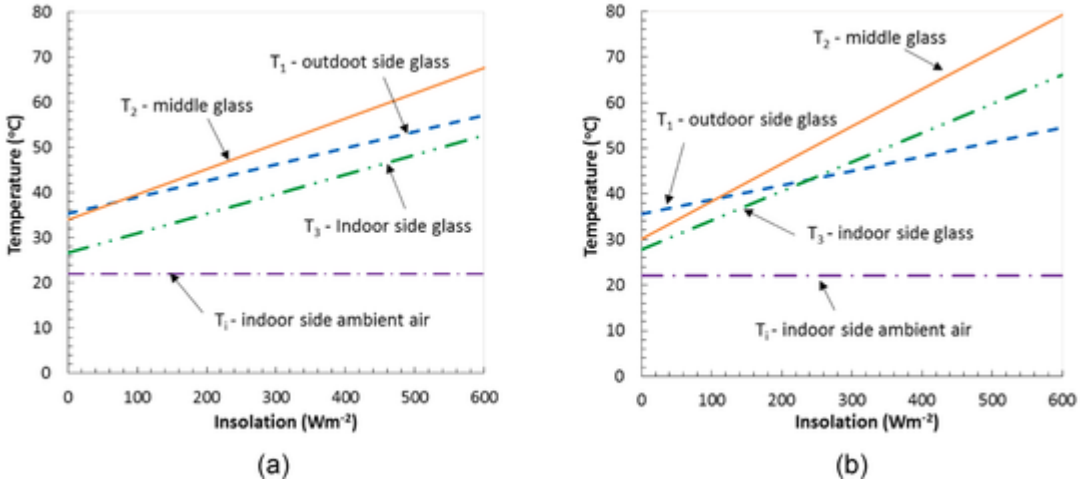

Fig. 9. Surface temperatures of the three glass sheets of (9a) IVW_{warm} and (9b) IVW_{cold} subjected to various solar insolation.

gain. STPV will work at a higher energy transfer efficiency due to lower glass temperature where the STPV is integrated. In the summer time, the STPV should be set on the indoor (warm-side) of IVW_{warm}, since the temperature of indoor glass of IVW_{warm} is lower than that of IVW_{cold}, thus STPV will achieve a higher energy transfer efficiency, and IVW_{warm} can achieve a lower solar heat gain g-value, thus a lower cooling load compared to IVW_{cold}.

CRediT authorship contribution statement

Yueping Fang: Formal analysis. **Saim Memon:** Formal analysis. **Jingqing Peng:** Formal analysis. **Mark Tyrer:** Formal analysis. **Tingzhen Ming:** Writing - review & editing.

Declaration of competing interest

This work funded by the Pump-Prime project of Coventry University and the self-initiated UK China industrial research collaboration is original research which is the further development of our previous research work, does not conflict with the interest of any third parties.

Acknowledgement

This work was supported by the Pump-Prime project (Ref: 13455-28) of Coventry University, InnovateUK project-ICURe grant (Ref:13-14/518470120) 2018..

References

[1] M.H. Wu, T.S. Ng, M.R. Skitmore, Sustainable building envelope design by considering energy cost and occupant satisfaction, Energy Sustain. Dev. 31 (2016) 118–129.
[2] D. D'Agostino, L. Mazzarella, What is a Nearly zero energy building? Overview, implementation and comparison of definitions, J. Build. Eng. 21 (2019) 200–212 2.
[3] S. Memon, Analysing the potential of retrofitting ultra-low heat loss triple vacuum glazed windows to an existing UK solid wall dwelling, Int. J. Renew. Energy Dev. 3 (3) (2014) 161.
[4] Y. Fang, T.J. Hyde, F. Arya, N. Hewitt, P.C. Eames, B. Norton, S. Miller, Indium alloy-sealed vacuum glazing development and context, Renew. Sustain. Energy Rev. 37 (2014) 480–501.
[5] Y. Fang, T. Hyde, N. Hewitt, P.C. Eames, B. Norton, Comparison of vacuum glazing thermal performance predicted using two-and three-dimensional models and their experimental validation, Sol. Energy Mater. Sol. Cells 93 (9) (2009) 1492–1498.
[6] P.C. Eames, Vacuum glazing: current performance and future prospects, Vacuum 82 (7) (2008) 717–722.
[7] P.W. Griffiths, P.C. Eames, T.J. Hyde, Y. Fang, B. Norton, Experimental characterization and detailed performance prediction of a vacuum glazing system fabricated with a low temperature metal edge seal, using a validated computer model, J. Sol. Energy Eng. 128 (2) (2006) 199–203.
[8] EN ISO 10077-1, Thermal Performance of Windows, Doors, and Shutters – Calculation of Thermal Tramsmittance –part 1: Simplified Method, European Committee for standardization (CEN), Brussels, 2017.
[9] S. Memon, Y. Fang, P.C. Eames, The influence of low-temperature surface induction on evacuation, pump-out hole sealing and thermal performance of composite edge-sealed vacuum insulated glazing, Renew. Energy 135 (2019) 450–464.
[10] Y. Fang, P.C. Eames, B. Norton, T.J. Hyde, Experimental validation of a numerical model for heat transfer in vacuum glazing, Sol. Energy 80 (5) (2006) 564–577.
[11] R.E. Collins, T.M. Simko, Current status of the science and technology of vacuum glazing, Sol. Energy 62 (3) (1998) 189–213.
[12] J.F. Zhao, P.C. Eames, T.J. Hyde, Y. Fang, J. Wang, A modified pump-out technique used for fabrication of low temperature metal sealed vacuum glazing, Sol. Energy 81 (9) (2007) 1072–1077.
[13] Collins and Fischer, Evacuated glazing, Sol. Energy 47 (1991) 27–38.
[14] S. Memon, Design, Fabrication and Performance Analysis of Vacuum Glazing Units Fabricated with Low and High Temperature Hermetic Glass Edge Sealing Materials PhD Thesis, Loughborough University, UK, 2013. https://dspace.lboro.ac.uk/2134/14562.
[15] S. Memon, F. Farukh, P.C. Eames, V.V. Silberschmidt, A new low-temperature hermetic composite edge seal for the fabrication of triple vacuum glazing, Vacuum 120 (2015) 73–82.
[16] S. Memon, P.C. Eames, Predicting the solar energy and space-heating energy performance for solid-wall detached house retrofitted with the composite edge-sealed triple vacuum glazing, Energy Procedia 122 (2017) 565–570.
[17] Y. Fang, T.J. Hyde, F. Arya, N. Hewitt, R. Wang, Y. Dai, Enhancing the thermal performance of triple vacuum glazing with low-emittance coatings, Energy Build. 97 (2015) 186–195.
[18] A. Ghosh, B. Norton, A. Duffy, Measured thermal performance of a combined suspended particle switchable device evacuated glazing, Appl. Energy 169 (2016) 469–480.
[19] S.D. Rezaei, S. Shannigrahi, S. Ramakrishna, A review of conventional, advanced, and smart glazing technologies and materials for improving indoor environment, Sol. Energy Mater. Sol. Cells 159 (2017) 26–51.
[20] H. Manz, S. Brunner, L. Wullschleger, Triple vacuum glazing: heat transfer and basic mechanical design constraints, Sol. Energy 80 (12) (2006) 1632–1642.
[21] Y. Fang, T.J. Hyde, F. Arya, N. Hewitt, A novel building component hybrid vacuum glazing - a modeling and experimental validation, ASHRAE Transact. 119 (2013) 430–441.
[22] Qingdao hengda glass technology co, ltd. 2019. Hd-glasscom[Online]. [15 May 2019]. Available from:http://www.hd-glass.com/en/about.aspx
[23] LandVac-Vacuum-glassnet, Vacuum-glassnet, 2019 [Online]. [10 April 2019]. Available from:. https://www.vacuum-glass.net/.
[24] Panasoniccom, Panasonic Newsroom Global, 2019 [Online]. [13 June 2019]. Available from:. http://news.panasonic.com/global/press/data/2017/12/en171205-2/en171205-2.html.
[25] NSG SPACIA, Pilkington NSG Hybrid Vacuum Glazing, 2019 [Online]. [23rd May 2019]. Available from:. https://www.nsg.com/en/media/ir-updates/announcements-2018/super-spacia-award.
[26] EN 673, Glass in Building – Determination of Thermal Transmittance (U-Value) –Calculation Method, European Committee for Standardization (CEN), Brussels, 2011.
[27] S. Memon, Experimental measurement of hermetic edge seal's thermal conductivity for the thermal transmittance prediction of triple vacuum glazing, Case Stud. Therm. Eng. 10 (2017) 169–178.
[28] J.A. Duffie, W.A. Beckman, Solar Engineering of Thermal Processes, Wiley, New York, 1991, pp. 770–772.